

Remarkably robust and correlated coherence and antiferromagnetism in $(\text{Ce}_{1-x}\text{La}_x)\text{Cu}_2\text{Ge}_2$

H. Hodovanets^{1,2}, S. L. Bud'ko^{1,2}, W. E. Straszheim¹, V. Taufour^{1,2}, E. D. Mun², H. Kim², R. Flint^{1,2}, and P. C. Canfield^{1,2}

¹*Ames Laboratory, Iowa State University, Ames, Iowa 50011, USA and*

²*Department of Physics and Astronomy, Iowa State University, Ames, Iowa 50011, USA*

We present magnetic susceptibility, resistivity, specific heat, and thermoelectric power measurements on $(\text{Ce}_{1-x}\text{La}_x)\text{Cu}_2\text{Ge}_2$ single crystals ($0 \leq x \leq 1$). With La-substitution, the antiferromagnetic temperature T_N is suppressed in an almost linear fashion and moves below 0.36 K, the base temperature of our measurements for $x > 0.8$. Remarkably, in addition to robust antiferromagnetism, the system also shows low temperature coherent scattering below T_{coh} up to ~ 0.9 of La, indicating a small percolation limit $\sim 9\%$ of Ce that separates a coherent regime from a single-ion Kondo impurity regime. T_{coh} as a function of magnetic field was found to have different functional dependencies in coherent and single-ion regimes. Remarkably, $(T_{coh})^2$ was found to be linearly proportional to T_N . The jump in the magnetic specific heat δC_m at T_N as a function of T_K/T_N for $(\text{Ce}_{1-x}\text{La}_x)\text{Cu}_2\text{Ge}_2$ follows the theoretical prediction based on the molecular field calculation for the $S = 1/2$ resonant level model.

PACS numbers: 71.10.Hf, 71.27.+a, 72.15.Qm, 75.20.Hr, 75.30.Kz, 75.30.Mb

In diluted Kondo alloys the magnetic impurities are randomly distributed and noninteracting and the Kondo effect occurs independently at each site. Physical properties of such alloys are governed by the characteristic Kondo temperature T_K . Once the amount of magnetic impurities, *e.g.* Ce ions, is increased, they form a dense periodic sublattice of Ce ions, Kondo lattice, with more complex behavior compared to that of a dilute Kondo alloy. The interactions between the f electrons in $4f$ -based Kondo lattice systems are no longer negligible and more elaborate theoretical models are required to describe their properties. Theories developed for the single-ion Kondo impurity were successfully used to describe the properties of very diluted as well as coherent regimes of the Kondo lattice. For example, $(\text{Ce}_x\text{La}_{1-x})\text{Pb}_3$ shows remarkable single-ion Kondo scaling for a wide range of x and T (for these concentrations T_K is the same)[1, 2] and in the study of La dilution of the Kondo lattice compound, CeNi_2Ge_2 , remarkable single-ion Kondo scaling in the coherent Fermi-liquid regime as well as diluted regimes was found.[3] Therefore, a study of La diluted Kondo-lattice system is often helpful in understanding of physics of the Kondo-lattice itself. In addition, studies of diluted systems are useful for separating out the coherent (lattice) from incoherent (dilute) effects.

In this work, La dilution of the Kondo lattice compound CeCu_2Ge_2 , $T_N \sim 4$ K[4–6], has been studied using magnetization, specific heat, resistivity, and thermoelectric power measurements with the hope of learning how the coherent state of the Kondo lattice evolves into the single-ion Kondo state upon La dilution. We found that upon La substitution T_N of $(\text{Ce}_{1-x}\text{La}_x)\text{Cu}_2\text{Ge}_2$ is suppressed in an almost linear fashion and moves below 0.36 K for $x > 0.8$. Remarkably, in addition to robust AFM order, the system also shows low temperature co-

herent scattering below T_{coh} up to ~ 0.9 of La, indicating a small percolation threshold, so that $\sim 9\%$ of Ce separates a low-temperature coherent regime from a single-ion Kondo impurity regime. T_{coh} as a function of magnetic field was found to have different functional dependencies in coherent and single-ion Kondo regimes.

The measurements were performed on single crystals grown by the high temperature flux method.[7, 8] The actual concentrations of La or Ce were assessed by wavelength dispersive x-ray spectroscopy (WDS) and the results of the Curie-Weiss fits of the temperature dependent susceptibility. The WDS values of La/Ce concentrations will be used throughout the text if not specified otherwise. La concentrations will be denoted by x and Ce concentrations will be denoted by $y=1-x$ to avoid confusion. The details of samples growth, evaluation of La concentrations and measurement techniques can be found in the Supplementary Material [9].

An almost classic, mean-field-like second order AFM transition is clearly seen in the specific heat $C_p(T)$ data for CeCu_2Ge_2 (Fig. 1). As the amount of La is increased, the AFM transition moves to lower temperature and is still clearly observable for $x = 0.80$. When T_N is suppressed enough, in addition to the AFM ordering, a broad maximum appears in the specific heat data starting from $x = 0.75$ (inset to Fig. 1), the position of which shifts slightly to lower temperatures as the La concentration is further increased. The maximum becomes almost indiscernible for $x = 0.99$. This maximum is associated with the Kondo temperature T_K of a single-ion Kondo impurity ($T_K > T_N$).[9]

A hallmark of the single-ion Kondo effect is the minimum and lower-temperature logarithmic dependence of the resistivity data. The zero-field, temperature dependent, in-plane, resistivity $\rho(T)$ data of

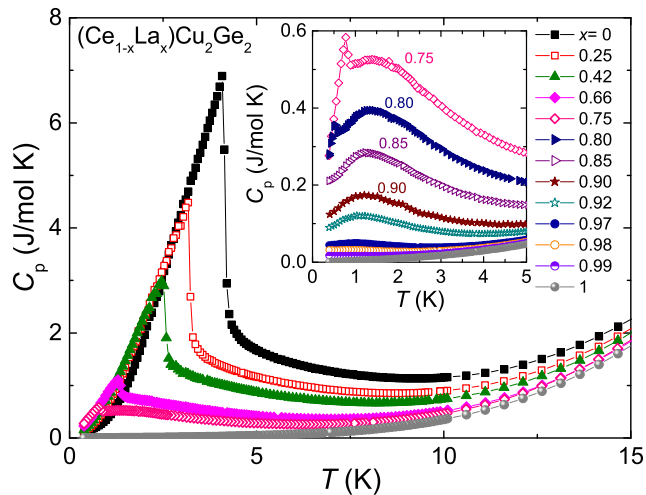


FIG. 1: Specific heat $C_p(T)$ data of $(\text{Ce}_{1-x}\text{La}_x)\text{Cu}_2\text{Ge}_2$ single crystals. The inset shows the enlarged low-temperature data for $0.75 \leq x \leq 1$. The data for $x = 0.75$ are shown in both graphs for clarity.

$(\text{Ce}_{1-x}\text{La}_x)\text{Cu}_2\text{Ge}_2$ are shown on a semi-logarithmic plot in Fig. 2. For CeCu_2Ge_2 , the $\rho(T)$ data exhibit a broad maximum at ~ 100 K associated with a thermal depopulation of the excited CEF levels[10] as the temperature is decreased. At lower temperatures, the $\rho(T)$ plot shows a second broad maximum corresponding to a crossover from incoherent to coherent scattering of the electrons on the magnetic moments at $T_{coh} \sim 5.5$ K, characteristic of that of Kondo lattice compounds. The maximum is followed by (and actually truncated by) a kink corresponding to the AFM transition. As the amount of La is increased, the AFM transition moves to lower temperatures. The kink, corresponding to the AFM transition, becomes less discernible. Most intriguingly, the truncated maximum, at T_{coh} for CeCu_2Ge_2 , evolves into a broad maximum and remains present up to $x = 0.9$, Fig. 2(b). For $x = 0.92$, the resistivity data tend to saturation at the lowest temperature measured. This behavior in the resistivity is reminiscent of the single-ion Kondo impurity. For the three smallest Ce concentrations, the resistivity data display the minimum followed by a $-\log(T)$ dependence upon cooling to the lowest temperature. It is worth pointing out that the slightly temperature dependent minimum at ~ 20 K in the resistivity data is observed for all samples containing Ce. T_{min} is proportional to the concentration of Ce, $y^{1/5}$, only for $0.01 \leq y \leq 0.08$ (see Supplemental Material [9]) consistent with the single-ion Kondo impurity effect.

Thermoelectric power (TEP) can also provide information about the T_{coh} and T_K characteristic energy scales. Temperature-dependent thermoelectric power $S(T)$ data for $(\text{Ce}_{1-x}\text{La}_x)\text{Cu}_2\text{Ge}_2$ single crystals are shown in Fig. 3. The broad peak observed for LaCu_2Ge_2 at ~ 75 K ($\sim 0.2 \times \Theta_D$) is probably due to the phonon drag con-

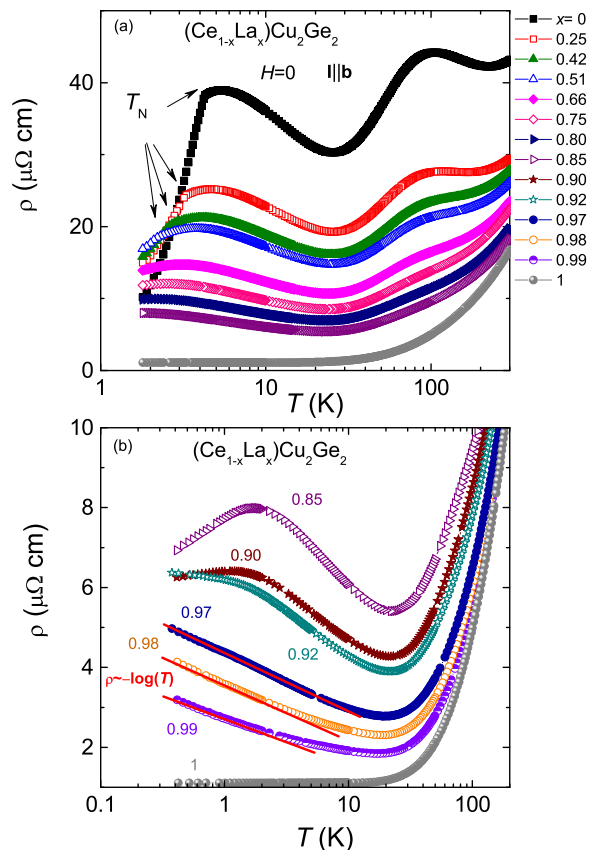


FIG. 2: (a) and (b) The zero-field, in-plane ($I \parallel b$), temperature-dependent resistivity $\rho(T)$ data of $(\text{Ce}_{1-x}\text{La}_x)\text{Cu}_2\text{Ge}_2$ single crystals on a semi-logarithmic plot. The data for $x = 0.85$ is shown in both panels for continuity.

tribution expected at $0.1-0.3\Theta_D$ [11]. For all samples containing Ce, a broad, high- T maximum due to the thermal depopulation of the two excited CEF doublets [10] as the temperature is lowered and possibly phonon drag contribution is observed around 100 K. It is worth recalling that the two excited CEF levels for CeCu_2Ge_2 are at $\Delta E_1 \sim 197$ K and $\Delta E_2 \sim 212$ K from the ground state doublet.[10] Since the energy separation between those two excited CEF levels is small, only one maximum at high temperatures is seen in the TEP measurements. The position of this maximum is almost unaffected by La substitution.

The TEP data of LaCu_2Ge_2 are positive over the whole temperature range measured. However, 0.01 of Ce is enough to change the functional dependence of the TEP below ~ 24 K: the TEP for $x = 0.99$ crosses zero twice by going through a low-T minimum and has a low-T maximum at ~ 0.6 K (see inset to Fig. 3). Such TEP behavior is expected for Ce single-ion Kondo impurity.[12–14] For the very La diluted samples, this low-temperature maximum is believed to correspond to the single-ion impurity Kondo temperature T_K . As the amount of Ce is increased, the absolute value of S_{min} increases as well

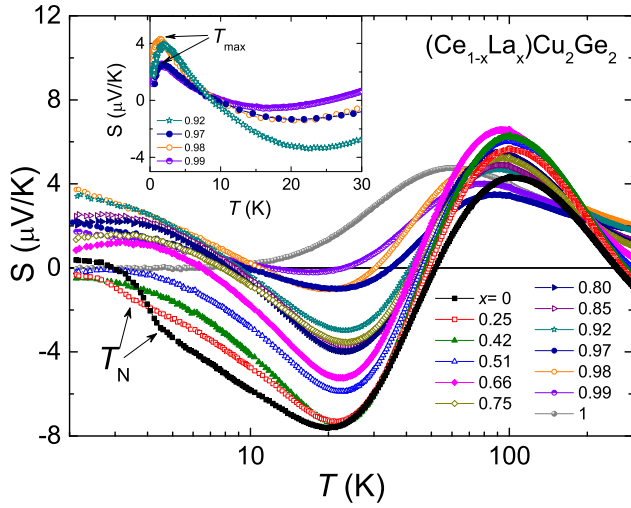


FIG. 3: The zero-field, temperature-dependent thermoelectric power $S(T)$ of $(\text{Ce}_{1-x}\text{La}_x)\text{Cu}_2\text{Ge}_2$ single crystals. $S(T)$ of $(\text{Ce}_{1-x}\text{La}_x)\text{Cu}_2\text{Ge}_2$ ($0.92 \leq x \leq 1$) single crystals at lower temperatures is shown in the inset. $\nabla T \parallel \mathbf{b}$.

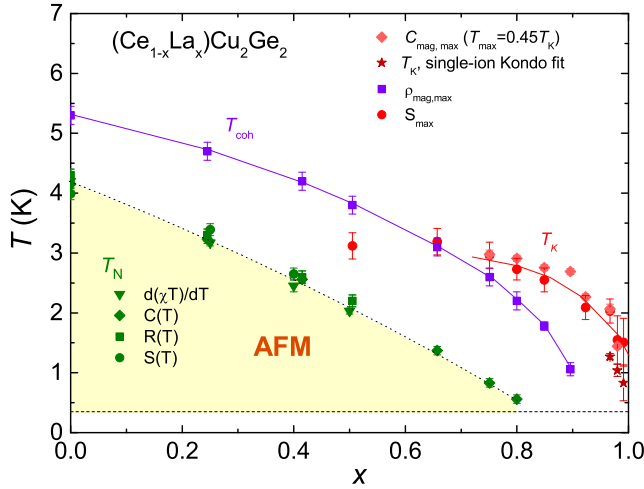


FIG. 4: $T-x$ phase diagram for $(\text{Ce}_{1-x}\text{La}_x)\text{Cu}_2\text{Ge}_2$ single crystals. Lines are guides to the eye. The horizontal line at 0.36 K is the lowest base temperature of the measurements. The data for magnetization measurements and T_K -values, estimated using Schotter and Schotter model of the specific heat data, can be found in the Supplemental Material [9]. Kondo temperature T_K was also estimated from the specific heat data by using $T_{max} = 0.45 T_K$ criterion [17] (see text for details).

probably reflecting the amount of Ce ions and increased scattering associated with the increase of Ce.

The $T-x$ phase diagram for $(\text{Ce}_{1-x}\text{La}_x)\text{Cu}_2\text{Ge}_2$, Fig. 4, shows the characteristic temperatures and energy scales as a function of La concentration. T_N (as determined from specific heat, magnetization, resistivity and TEP measurements) decreases almost linearly with x and moves below the base temperature of 0.36 K for $x > 0.80$. The presence of the AFM transition and linear dependence of it on x to a high value of La is not unique to

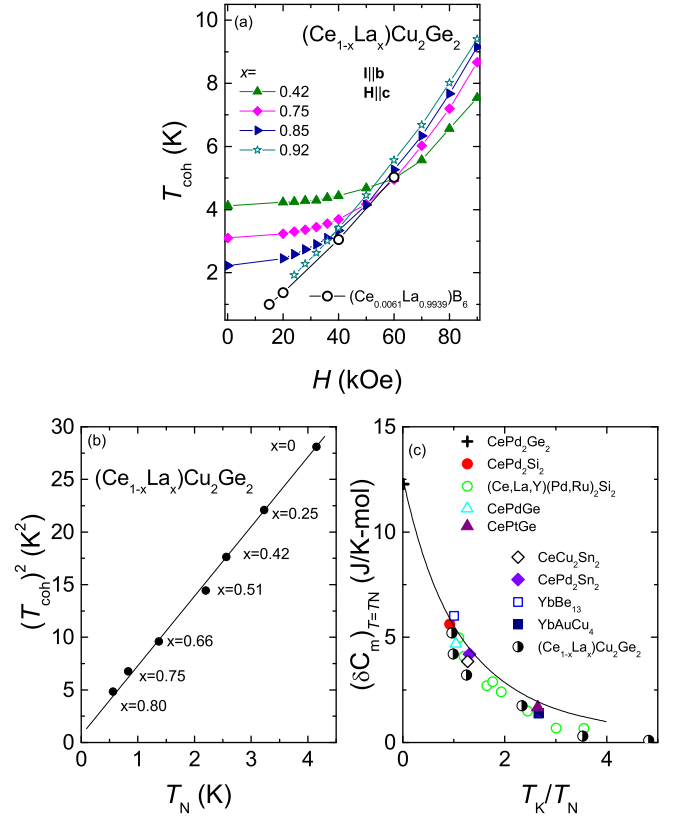


FIG. 5: (a) T_{coh} as a function of H . The data for 0.61 % of Ce in LaB_6 were estimated from the $\rho(T)$ data presented in Ref. 20. (b) $(T_{coh})^2$ as a function of T_N . Solid line is a guide to the eye. (c) Variation of the jump in the specific heat δC_m at the magnetic transition as a function of T_K/T_N . The data for the compounds not studied in this work together with the solid curve were digitized from Ref. [21]. Solid line is the calculated specific heat jump at the T_N for a doublet ground state system.[21]

$(\text{Ce}_{1-x}\text{La}_x)\text{Cu}_2\text{Ge}_2$ system. Such behavior of T_N upon La-dilution was also observed in $(\text{Ce}_{1-x}\text{La}_x)\text{Pd}_2\text{Si}_2$ [15], as well as in $(\text{Ce}_{1-x}\text{La}_x)\text{Au}_2\text{Si}_2$, and $(\text{Ce}_{1-x}\text{La}_x)\text{Ag}_2\text{Si}_2$ [16]. Ce-based parent compounds of these families, including CeCu_2Ge_2 , order antiferromagnetically, with different ordering wave vectors, and belong to the same $I4/mmm$ space group of the tetragonal crystal structure. However, a progression of the T_{coh} , that corresponds to the crossover from incoherent to coherent scattering, with La substitution was not commented on for these systems, perhaps because T_N and T_{coh} could not be well separated. In this respect, $(\text{Ce}_{1-x}\text{La}_x)\text{Cu}_2\text{Ge}_2$ appears to be a unique system – the T_{coh} is well separated from the AFM feature and extends all the way to ~ 0.9 of La.

The low-temperature maxima in the TEP data seem to coincide with the T_K -values estimated from the specific heat data using a $T_{max} = 0.45 T_K$ criterion [17] rather well, here T_{max} is the temperature where the maximum occurs. The T_K values estimated using the single-ion Kondo model Schotte and Schotte fit [9, 18] of the specific

heat data seem to be lower than the ones obtained using the aforementioned criterion, however, they fall within the error bars of the ones estimated using the $T_{max} = 0.45 T_K$, criterion.

The observation of T_N and T_{coh} down to small values of Ce, can be explained by the percolation limit of the lattice of Ce ions being rather small so that just $\sim 9\%$ of Ce separates the low-temperature coherent and single ion regimes. In the single-ion Kondo limit, the Kondo screening clouds of different Ce do not overlap or significantly interact, but once the amount of Ce is increased to a sufficient number for the Kondo screening clouds to overlap, where “sufficient” is determined by the percolation threshold, the system will develop Kondo coherence. The percolation threshold can tell us a lot about the Kondo cloud size and dimensionality. The 9% threshold rules out a 2D network and indeed requires further neighbors overlaps even in the 3D case, where a cubic lattice with second and third nearest neighbors gives percolation threshold of 0.0976 [19]. Once coherence is established, the system can develop an AFM transition. At a more qualitative level, given that the clear AFM ordering signatures persist out to $x = 0.8$, indicating that there is clear coupling and interaction between the remains of the Ce-sublattice, it is not at all surprising that this same coupling and interactions support coherence between ions.

Different field-dependence of the T_{coh} in the coherent and single-ion regimes, Fig. 5(a), also supports the statement that $y \approx 9\%$ separates the coherent and single ion regimes in the zero-field limit (Fig. 5(a) is based on the data given in Supplementary Material [9]). The functional dependence of T_{coh} on H for $x = 0.92$ is different from that for smaller La concentrations and closely resembles that of 0.61% of Ce in LaB₆ [20] which is in the single-ion Kondo impurity regime.

Remarkably, $(T_{coh})^2$ was found to be linearly proportional to T_N , Fig. 5(b), over wide range of x and both seem to go to zero at $x \sim 0.9$. As of yet, there is no theory to explain a clear and compelling dependence of T_{coh} on T_N .

Based on the molecular field calculations for the $S = 1/2$ resonant level model, a close relationship between the specific heat jump, δC_m , at the ordering temperature and the ratio between the two characteristic temperatures T_K and T_N for magnetic Ce and Yb Kondo systems for a doublet ground state was found [21]. If the T_K -values shown in Fig. 4 are used and T_K for CeCu₂Ge₂ assumed 4 K, (Ce_{1-x}La_x)Cu₂Ge₂ fits that description rather well, Fig. 5(c). This further supports the thought that the estimated T_K values are reasonable and the CEF ground state is a doublet.

In summary, the parent CeCu₂Ge₂ compound orders antiferromagnetically below $T_N \sim 4$ K. La substitution drives T_N in a roughly linear fashion below 0.36 K, the base temperature of our measurements, for $x > 0.8$. How-

ever, T_{coh} , corresponding to the crossover from incoherent to coherent scattering, was observed up to $x \sim 0.9$. This indicates that the percolation limit of the lattice of Ce ions is rather small and implies the 3D nature of the Kondo “clouds”. $y \approx 9\%$ separates the coherent regime from the single ion regime. T_{coh} as a function of H was found to have different functional dependence in the coherent and single ion regimes. Remarkably, $(T_{coh})^2$ was found to be linearly proportional to T_N over wide range of x . The Kondo temperature was found to change in the non-linear fashion from ~ 4 K to ~ 1 K upon La substitution. This T_K decrease with x is consistent with the volume increase with x in terms of Doniach phase diagram. For $0.01 \leq y \leq 0.08$, T_{min} in the resistivity data is proportional to $y^{1/5}$ as expected for the single-ion Kondo impurity. The jump in the magnetic specific heat δC_m at T_N as a function of T_K/T_N for (Ce_{1-x}La_x)Cu₂Ge₂ follows the theoretical prediction for the molecular field calculations for the $S = 1/2$ resonant level model[21].

The authors would like to thank P. Riseborough, Z. Fisk, J. D. Thompson and F. Steglich for insightful discussions. This work was done at Ames Laboratory, US DOE, under contract #DE-AC02-07CH11358. This work was supported by the US Department of Energy, Office of Basic Energy Science, Division of Materials Sciences and Engineering. E.D. M and H. K. were supported by the AFOSR-MURI grant No. FA9550-09-1-0603.

-
- [1] C. L. Lin, A. Wallash, J. E. Crow, T. Mihalisin, and P. Schlottmann, Phys. Rev. Lett. **58**, 1232 (1987).
 - [2] P. Schlottmann, Phys. Rep. **181**, 1 (1989).
 - [3] A. P. Pikul, U. Stockert, A. Steppke, T. Cichorek, S. Hartmann, N. Caroca-Canales, N. Oeschler, M. Brando, C. Geibel, and F. Steglich, Phys. Rev. Lett. **108**, 066405 (2012).
 - [4] U. Rauchschwalbe, U. Gottwick, U. Ahlheim, H. Mayer, and F. Steglich, J. Less Common Met. **111**, 265 (1985).
 - [5] R. Felten, G. Weber, and H. Rietschel, J. Magn. Mater. **63-64**, 383 (1987).
 - [6] F. de Boer, J. Klaasse, P. Veenhuizen, A. Bhm, C. Bredl, U. Gottwick, H. Mayer, L. Pawlak, U. Rauchschwalbe, H. Spille, et al., J. Magn. Mater. **63-64**, 91 (1987).
 - [7] P. C. Canfield and Z. Fisk, Phil. Mag. B **65**, 1117 (1992).
 - [8] P. C. Canfield, “Solution Growth of Intermetallic Single Crystals: A Beginner’s Guide”, in *Properties and Applications of Complex Intermetallics*, edited by E. Belin-Ferré (World Scientific, Singapore, 2010), Vol. 2, Chap. 2, p. 93.
 - [9] See Supplemental Material at.
 - [10] M. Loewenhaupt, E. Faulhaber, A. Schneidewind, M. Deppe, and K. Hradil, J. Appl. Phys. **111**, 07E124 (2012).
 - [11] F. J. Blatt, P. A. Schroeder, C. L. Foiles, and D. Greig, *Thermoelectric Power of Metals* (Plenum Press, New York, 1976).
 - [12] V. Zlatić, B. Horvatić, I. Milat, B. Coqblin, G. Czycholl, and C. Grenzbach, Phys. Rev. B **68**, 104432 (2003).

- [13] V. Zlatić and R. Monnier, Phys. Rev. B **71**, 165109 (2005).
- [14] V. Zlatić, R. Monnier, J. K. Freericks, and K. W. Becker, Phys. Rev. B **76**, 085122 (2007).
- [15] E. V. Sampathkumaran, Y. Nakazawa, M. Ishikawa, and R. Vijayaraghavan, Phys. Rev. B **40**, 11452 (1989).
- [16] C. Garde, J. Ray, and G. Chandra, J. Alloys and Compd. **198**, 165 (1993).
- [17] H.-U. Desgranges and K. Schotte, Phys. Lett. A **91**, 240 (1982).
- [18] K. Schotte and U. Schotte, Phys. Lett. A **55**, 38 (1975).
- [19] L. Kurzawski and K. Malarz, Rep. Math. Phys. **70**, 163 (2012).
- [20] K. Samwer and K. Winzer, Z. Phys. B: Condens. Matter **25**, 269 (1976).
- [21] M. Besnus, A. Braghta, N. Hamdaoui, and A. Meyer, J. Magn. Magn. Mater. **104-107, Part 2**, 1385 (1992).

Supplementary Material: Remarkably robust and correlated coherence and antiferromagnetism in $(\text{Ce}_{1-x}\text{La}_x)\text{Cu}_2\text{Ge}_2$

H. Hodovanets^{1,2}, S. L. Bud'ko^{1,2}, W. E. Straszheim¹, V. Taufour^{1,2},
E. D. Mun^{1,2}, H. Kim², R. Flint^{1,2}, and P. C. Canfield^{1,2}

¹Ames Laboratory, Iowa State University, Ames, Iowa 50011, USA and

²Department of Physics and Astronomy, Iowa State University, Ames, Iowa 50011, USA

Experimental

Single crystals of $(\text{Ce}_{1-x}\text{La}_x)\text{Cu}_2\text{Ge}_2$ were grown from a ternary solution rich in Cu-Ge self-flux. The detailed description of the growth from the ternary melt can be found in Ref. [1–3]. A starting composition of $(\text{Ce}_{1-x}\text{La}_x)_{0.05}\text{Cu}_{0.475}\text{Ge}_{0.475}$ was placed in a 2-ml alumina crucible, sealed in a silica ampule under a small partial pressure of high purity argon gas. The ampule was heated to 1180 °C, dwelled there for 2 h, then cooled over 155 h to 825 °C, at which temperature the excess liquid was decanted using a centrifuge. To prepare the samples with nominal concentration of Ce, $y = 1 - x$, in the range $0.01 \leq y \leq 0.08$, a master ingot of $(\text{Ce}_{0.08}\text{La}_{0.92})_{0.05}\text{Cu}_{0.475}\text{Ge}_{0.475}$ was prepared first by arc-melting. Then, parts of the master ingot and $\text{La}_{0.05}\text{Cu}_{0.475}\text{Ge}_{0.475}$ were mixed in the ratios of 1:1, 1:2, and 1:4 to get the nominal values of $y = 0.04, 0.02$, and 0.01 , respectively. The single crystals grow as plates with the tetragonal c -axis perpendicular to the plate and the Laue back-reflection pattern (not shown here) confirmed that the plate-like samples have edges along (100) or (010) with the c -axis perpendicular to the plates.

The actual (as opposed to nominal) La concentration was determined in two ways (i) by wavelength dispersive x-ray spectroscopy (WDS) in a JEOL JXA-8200 electron microprobe and (ii) based on the results of the

Curie-Weiss fit. Figure S1(a) presents the results of both approaches. The modified Curie-Weiss law fit $\chi = \chi_0 + yC/(T - \theta)$ of the polycrystalline average $\chi_{ave} = (2\chi_a + \chi_c)/3$ was performed in 150 K $< T < 300$ K range. y is Ce concentration and $y = 1 - x$. $C = (N_A p_{eff}^2)/3k_B$, $p_{eff} = 2.54\mu_B$ is the expected effective moment for the Ce^{3+} , μ_B is the Bohr magneton, N_A is the Avogadro number, and k_B is the Boltzmann constant. Before the fit was performed, the $M(T)/H$ data of polycrystalline average of LaCu_2Ge_2 were subtracted. The agreement between these two ways of estimation of Ce concentrations is quite good, especially for larger amounts of Ce, Fig. S1(b). Clearly, uncertainty at the $\Delta y = 0.01 - 0.02$ level becomes very large in terms of the y value as y becomes smaller than 0.2 or 0.1. On the other hand, the linearity of the $x - x_{nominal}$ plot is consistent with complete solubility of Ce in La for this structure. The WDS values of La concentrations will be used throughout the text if not specified otherwise.

Powder x-ray diffraction (XRD) data were collected on a Rigaku MiniFlex diffractometer (using $\text{Cu } K_{\alpha 1,2}$ radiation) at room temperature. The x-ray measurements confirmed $I4/mmm$ crystal structure of the samples. Lattice parameters were refined by the LeBail method using Rietica software. Figure S2 shows the evolution of the lattice parameters a and c and a unit cell volume V with increasing of La content. La-substitution results in the slight decrease of the value of c (0.1%) and increase of a (1.1%) lattice parameters. The unit cell volume V increases with La substitution: $V(\text{LaCu}_2\text{Ge}_2)$ is 2 % larger than $V(\text{CeCu}_2\text{Ge}_2)$.

Magnetic measurements were carried out in a Quantum Design Magnetic Property Measurement System (MPMS) SQUID magnetometer. For the measurements with $\mathbf{H} \parallel \mathbf{a}$, magnetic field along the plate, the samples were mounted in between two transparent plastic straws [4]. For the magnetic field applied along the c -axis, perpendicular to the plates, the samples were mounted in the transparent plastic straws with two additional plastic straws holding the samples in place. This latter technique leads to the gap in the straw with a paramagnetic contribution to the total magnetic signal. The temperature dependence of the magnetization of the gap is almost temperature independent above ~ 50 K, which contributes to the χ_0 value, and linear magnetic field dependence. For the smallest Ce concentration, the fused silica

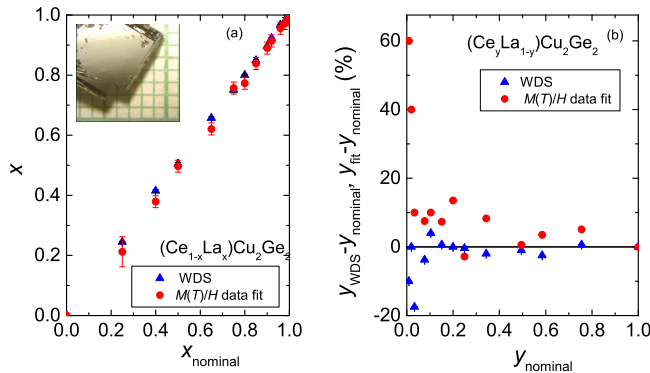


FIG. S1: (a) La-concentrations of $(\text{Ce}_{1-x}\text{La}_x)\text{Cu}_2\text{Ge}_2$ single crystals, as determined by wavelength dispersive spectroscopy WDS and Curie-Weiss law fit of $M(T)/H$ data, versus nominal La-values. The inset shows large and shiny single crystal from the series. (b) Difference between the values obtained by WDS and Curie-Weiss law fit and nominal values as a function of Ce concentration, y .

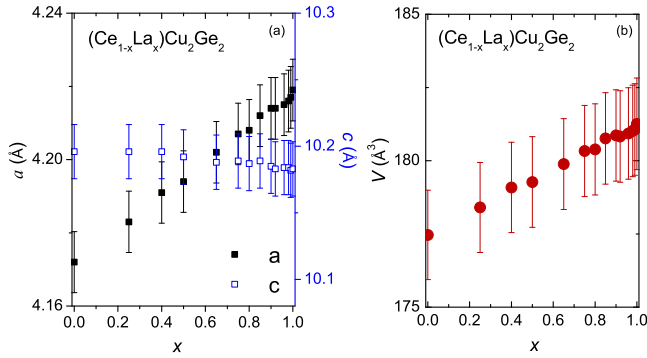


FIG. S2: (a) Lattice parameters a and c , and (b) the unit cell volume V as a function of La concentration of $(\text{Ce}_{1-x}\text{La}_x)\text{Cu}_2\text{Ge}_2$ single crystals.

rod with the gap in the middle was used for the magnetization measurements. The temperature and field dependent magnetization of the fused silica rod was measured beforehand to allow for the appropriate background subtraction.

Transport and specific heat measurements were performed in a Quantum Design Physical Property Measurement System PPMS-14 with ^3He option and PPMS-9. A standard four-probe geometry, ac technique ($f=16$ Hz, $I=3-1$ mA) was used to measure the electrical resistance of the samples. Electrical contact to the samples was made with platinum wires attached to the samples using EpoTek H20E silver epoxy. The care was taken to prepare the samples for the resistivity measurements so that the current was flowing along the edge of the plates, current along a (100)-direction. To calculate the resistivity of samples the distance between the midpoint of two voltage contacts and the cross-section area of the samples were used.

For the specific heat measurements, a relaxation technique with fitting of the whole temperature response of the microcalorimeter was utilized. The background specific heat that includes sample platform and grease was measured for all necessary temperature values (in some instances magnetic field values as well) and subtracted from the total specific heat. The specific heat of LaCu_2Ge_2 was measured in the same temperature range and was used to estimate a phonon and “non-correlated” electronic contributions to the specific heat of $(\text{Ce}_{1-x}\text{La}_x)\text{Cu}_2\text{Ge}_2$ single crystals.

The thermoelectric power (TEP) measurements were performed by a dc , alternating temperature gradient $\nabla T \parallel \mathbf{b}$ (two heaters and two thermometers) technique [5] with the temperature environment between 2 and 300 K provided by a Quantum Design PPMS. The samples were mounted with the help of Du-Pont 4929N silver paste directly on the surfaces of the SD packages of Cernox thermometers. The silver paste ensures thermal and elec-

trical contact. The TEP measurements were extended down to ~ 0.5 K by utilizing CRYO Industries of America, Inc. ^3He cryostat. In this case, the samples were mounted on the surfaces of the SD packages of Cernox thermometers with the silver epoxy and were allowed to cure at $\sim 70^\circ\text{C}$ for about one hour.

Magnetization measurements

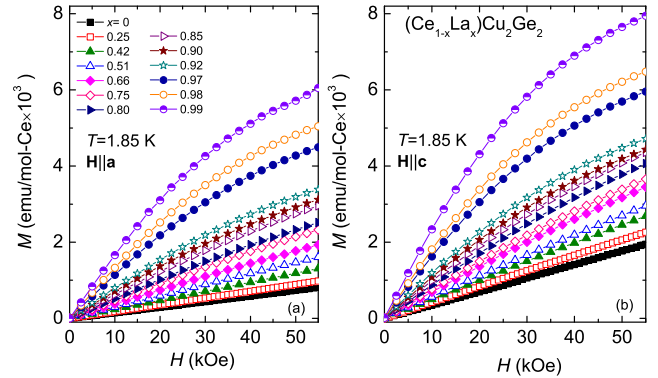


FIG. S3: M per mole of Ce versus H at 1.85 K of $(\text{Ce}_{1-x}\text{La}_x)\text{Cu}_2\text{Ge}_2$ single crystals (a) $\mathbf{H} \parallel \mathbf{a}$ and (b) $\mathbf{H} \parallel \mathbf{c}$.

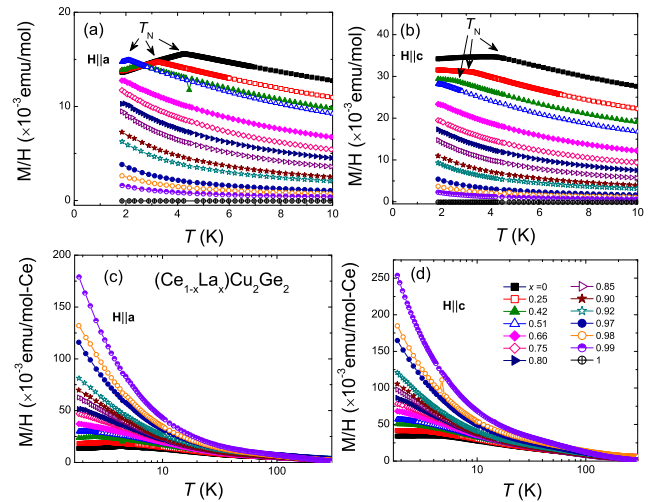


FIG. S4: $M(T)/H$ of $(\text{Ce}_{1-x}\text{La}_x)\text{Cu}_2\text{Ge}_2$ single crystals (a) and (c) $\mathbf{H} \parallel \mathbf{a}$; (b) and (d) $\mathbf{H} \parallel \mathbf{c}$. For all samples containing Ce, a magnetic field of $H = 1$ kOe was used to collect the data. For LaCu_2Ge_2 , the field of $H = 10$ kOe was used to collect the data. Panels (c) and (d) show the data, with $M(T)/H$ data of LaCu_2Ge_2 subtracted, in units of emu/mol-Ce , as opposed to emu/mol shown in panels (a) and (b). Hence, panels (c) and (d) do not have the data for $x = 1$. Since the same, assigned to each concentration, symbols were followed in four panels, all legends are listed once in panel (d) for convenience.

Figure S3 shows magnetic isotherms $M(H)$ at $T = 1.85$ K. $M(H)$ data were taken with the magnetic field applied

along the a - and c - axes. The $M(H)$ data of LaCu_2Ge_2 were subtracted from each curve in an attempt to account for non- $4f$ -shell related background. The magnetization for the field along the c -axis is larger than that for $\mathbf{H}\parallel\mathbf{a}$ even for the smallest amount of Ce.

$M(H)$ data for $0 \leq x \leq 0.51$ manifest linear field dependence up to 55 kOe, except for $x = 0.51$, $\mathbf{H}\parallel\mathbf{c}$, where it deviates slightly from linearity. For higher La level samples, as the amount of La increases, the $M(H)$ data show a tendency to saturation at higher fields.

Figure S4 shows $M(T)/H$ for $(\text{Ce}_{1-x}\text{La}_x)\text{Cu}_2\text{Ge}_2$ single crystals for the magnetic field applied along the a - and c - axes. The AFM ordering for $0 \leq x \leq 0.51$ can be seen as a kink, much sharper for $\mathbf{H}\parallel\mathbf{a}$, that moves to lower temperature as the amount of La increases. The magnetization for $\mathbf{H}\parallel\mathbf{c}$ is larger than that for $\mathbf{H}\parallel\mathbf{a}$, consistent with $M(H)$ data shown in Fig. S3, with the difference being most pronounced at lower temperatures.

Specific heat measurements

The low temperature linear fit of the C/T vs T^2 of LaCu_2Ge_2 results in $\gamma = 4 \text{ mJ mol}^{-1}\text{K}^{-2}$ ($3.6 \text{ mJ mol}^{-1}\text{K}^{-2}$ was estimated based on the electronic structure calculations [6]) and $\Theta_D = 350 \text{ K}$. Due to the AFM transition at $\sim 4 \text{ K}$, a γ value is hard to estimate precisely for CeCu_2Ge_2 . The low temperature linear fit over 24 to 30 K temperature range of the C/T vs T^2 of CeCu_2Ge_2 results in $\gamma \approx 90 \text{ mJ mol}^{-1}\text{K}^{-2}$ and the value of C_p/T at 0.39 K is $245 \text{ mJ mol}^{-1}\text{K}^{-2}$.

To check the origin of the maximum in the specific heat, the $C_{mag}(T)$ data at various constant magnetic fields were collected for $x = 0.85$, Fig. S5. These data can be compared with several possibilities:

(1) If the maximum in the specific heat is due to the first excited CEF level, then the application of the magnetic field results in the Zeeman splitting of the doublet which broadens the maximum.[7] However, according to the specific heat [8] and neutron scattering [9] measurements, the CEF splits the $J = \frac{5}{2}$ multiplet into three doublets with the first and second excited states being at $\Delta E_1 \sim 197 \text{ K}$ and $\Delta E_2 \sim 212 \text{ K}$ with respect to the ground state doublet. This rules out a Schottky anomaly in $C(T)$ data at low temperatures in zero field.

(2) In the case of spin glass state, the maximum in the specific heat is expected to broaden, decrease in height and move to higher temperatures upon application of magnetic field.[10] Although the feature does move up in temperature as the magnetic field is increased, it also increases in height, this means that the spin-glass state is also unlikely.

(3) If the maximum in the specific heat is due to the single-ion Kondo effect, then upon application of magnetic field, as the magnetic field becomes comparable and larger than the energy $k_B T_K$, the specific

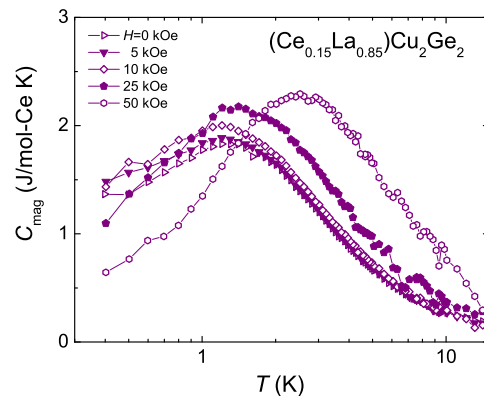


FIG. S5: $C_{mag}(T)$ data of $(\text{Ce}_{0.15}\text{La}_{0.85})\text{Cu}_2\text{Ge}_2$ single crystal for various applied magnetic fields.

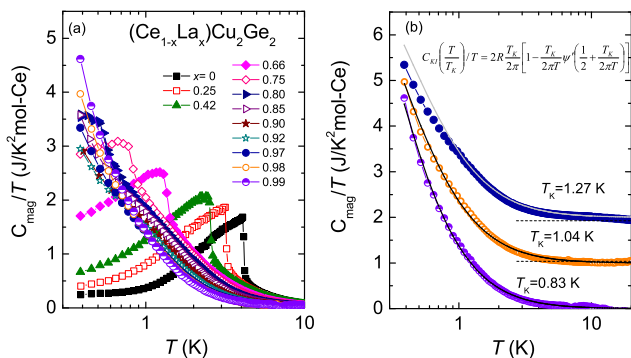


FIG. S6: (a) C_{mag}/T versus T data normalized by the amount of Ce of $(\text{Ce}_{1-x}\text{La}_x)\text{Cu}_2\text{Ge}_2$ single crystals. (b) Fit of Kondo resonance model by Schotte and Schotte [15] for 1 mole of the Kondo impurity with the effective spin $S = \frac{1}{2}$. T_K is the Kondo temperature defined as the width of the Lorentzian-shape Kondo resonance at the Fermi level. Each data set was offset from previous by $1 \text{ JK}^{-2}(\text{mol-Ce})^{-1}$ for clarity. Legends: \bullet $x = 0.97$, \circ $x = 0.98$, and half open circle $x = 0.99$.

heat peak becomes narrower and sharper and moves to higher temperatures.[11] Thus, the specific heat data of $(\text{Ce}_{0.15}\text{La}_{0.85})\text{Cu}_2\text{Ge}_2$, Fig. S5, show similar behavior to that of single-ion Kondo impurity. The maximum seen in the specific heat for other concentrations of La is most likely associated with the T_K of the single-ion Kondo impurity as well since La-substitution is not expected to drastically alter the CEF level scheme. Similar behavior of the maximum in the specific heat data upon application of magnetic field was observed for heavily La diluted CeB_6 [12], CeCu_6 [13], and CeAl_2 [14].

Figure S6(a) shows C_{mag}/T per mole of Ce atoms as a function of temperature for all samples measured. Again, a progression of the AFM ordering with the increase of La content is clearly seen for $x \leq 0.80$. For $0.97 \leq x \leq 0.99$, the $\gamma|_{0.4\text{K}}$ is rather large, indicating small Kondo temperature for these La concentrations. To check this assumption, the specific heat data were fitted based on

the Kondo impurity model. The Kondo impurity with the effective spin $S = \frac{1}{2}$ contribution to the specific heat per one mole of impurity according to the Kondo resonance model by Schotte and Schotte [15] is given by

$$C_{KI} = 2R \frac{T_K}{2\pi T} \left[1 - \frac{T_K}{2\pi T} \psi' \left(1 + \frac{T_K}{2\pi T} \right) \right],$$

where R is the universal gas constant, ψ' is the first derivative of the digamma function, and T_K is the Kondo temperature defined as the width of the Lorentzian-shape Kondo resonance at the Fermi level. The results of the fit to the C_{mag}/T vs T data for the three lowest Ce concentrations is given in Fig. S6 (b). T_K is the only fitting parameter. The model seems to describe the data rather well for $x = 0.99$ and 0.98 . However, for $x = 0.97$, this model does not describe the lowest temperature data well. Even worse fit (not shown here) is obtained for $x = 0.92$. The presence of additional magnetic contribution to the specific heat can be one of the possible reasons as to why the model does not describe the data well for the larger amounts of Ce.

Resistivity measurements

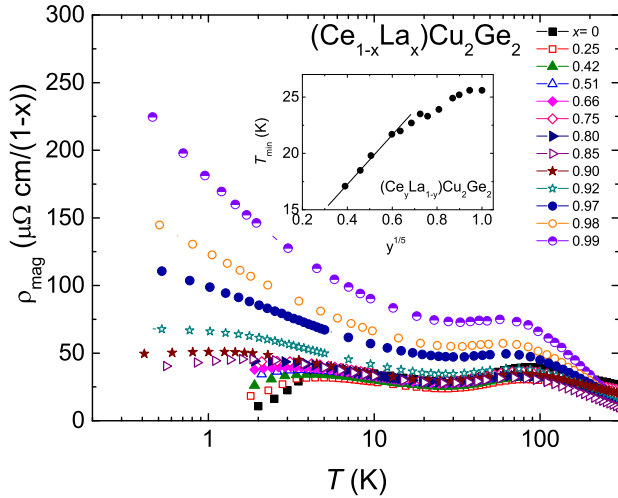


FIG. S7: The zero-field, temperature-dependent resistivity ($\mathbf{I}||\mathbf{b}$) $\rho(T)_{mag}$ data normalized to the Ce content of $(\text{Ce}_{1-x}\text{La}_x)\text{Cu}_2\text{Ge}_2$ single crystals on a semi-log plot. Every sixth data point is shown for clarity of the data presentation. The inset shows T_{min} as a function of $y^{1/5}$.

The magnetic contribution per Ce to the resistivity data ρ_{mag} is shown in Fig. S7. The data for $x \leq 0.90$ seem to fall onto a single manifold for $T > T_N$. However, the data for $x \geq 0.92$ show a clear departure from this trend. This behavior might be due to the greater variation of the T_K for $x \geq 0.92$ or the need to account for growing relative uncertainty in the Ce values. To account for this uncertainty, the x values for the four lowest La

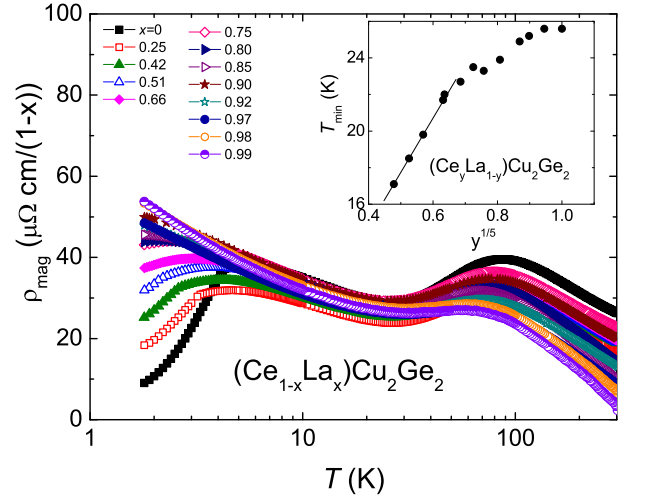


FIG. S8: The zero-field, temperature-dependent resistivity ($\mathbf{I}||\mathbf{b}$) $\rho(T)_{mag}$ data normalized to the Ce content of $(\text{Ce}_{1-x}\text{La}_x)\text{Cu}_2\text{Ge}_2$ single crystals on a semi-log plot. The four lowest Ce concentration were adjusted to $y = 0.025, 0.04, 0.06,$ and 0.10 instead of $y = 0.01, 0.02, 0.03,$ and 0.8 , the data of which are shown in Fig. S7, respectively. The inset shows T_{min} as a function of $y^{1/5}$ with the four smallest y values adjusted.

concentration were adjusted so that all data collapse onto one manifold and the result is shown in Fig. S8 together with the new graph of low-temperature T_{min} versus adjusted values of $y^{1/5}$, here y is concentration of Ce, that still holds for the new adjusted lowest concentrations of Ce. If these new values are adopted, then: (i) the $M(H)$ data at 55 kOe, shown in Fig. S3, and $M(T)/H$ data at lowest temperatures, Fig. S4, for these four lowest Ce concentrations fall in between the values of those for $0.42 \leq x \leq 0.80$; (ii) the fits of C_{mag}/T , shown in Fig. S6, do not describe the data very well any longer and result in $T_K = 0.15, 0.21,$ and 0.21 K starting from the smallest Ce concentration. If additional parameter that reflects Ce concentration is included in the Schotte and Schotter model, then original values of Ce concentrations and T_K -values shown in Fig. S6 are recovered. Therefore, for now, the analysis of the data will be based on the values of Ce obtained by the WDS analysis.

Resistivity in constant magnetic fields

The $\rho(T)$ data in constant magnetic fields, $\mathbf{H}||\mathbf{c}$, for $x = 0.42, x = 0.66, x = 0.80,$ and $x = 0.92$, are shown in Fig. S9. The $\ln T$ divergence of the resistivity at low temperatures is eliminated by the application of strong magnetic field. The strong magnetic field disallows spin-flip processes and causes a negative magnetoresistance.[16] The position of the T_{max} is shifting toward higher temperatures as the magnetic field is increased. The data presented in Fig. S9 were used to create Fig. 5(a) which describes the evolution of T_{max} or T_{coh} as a function of

magnetic field.

- [1] P. C. Canfield and Z. Fisk, *Phil. Mag. B* **65**, 1117 (1992).
- [2] P. C. Canfield, "Solution Growth of Intermetallic Single Crystals: A Beginner's Guide", in *Properties and Applications of Complex Intermetallics*, edited by E. Belin-Ferré (World Scientific, Singapore, 2010), Vol. 2, Chap. 2, p. 93.
- [3] P. C. Canfield and I. R. Fisher, *J. Crystal Growth* **225**, 155 (2001).
- [4] <http://www.qdusa.com/sitedocs/appNotes/mpms/1014-201.pdf>.
- [5] E. Mun, S. L. Bud'ko, M. S. Torikachvili, and P. C. Canfield, *Meas. Sci. Technol.* **21**, 055104 (2010).
- [6] G. Zwicknagl, *J. Low Temp. Phys.* **147**, 123 (2007).
- [7] H. Hodovanets, S. L. Bud'ko, X. Lin, V. Taufour, M. G. Kim, D. K. Pratt, A. Kreyssig, and P. C. Canfield, *Phys. Rev. B* **88**, 054410 (2013).
- [8] R. Felten, G. Weber, and H. Rietschel, *J. Magn. Magn. Mater.* **63-64**, 383 (1987).
- [9] M. Loewenhaupt, E. Faulhaber, A. Schneidewind, M. Deppe, and K. Hradil, *J. Appl. Phys.* **111**, 07E124 (2012).
- [10] J. Mydosh, *Spin Glasses: An Experimental Introduction* (Taylor & Francis Group, 1993).
- [11] P. Schlottmann, *J. Magn. Magn. Mater.* **52**, 214 (1985).
- [12] H. Gruhl and K. Winzer, *Solid State Commun.* **57**, 67 (1986).
- [13] K. Satoh, T. Fujita, Y. Maeno, Y. Ōnuki, and T. Komatsubara, *J. Phys. Soc. Jpn.* **58**, 1012 (1989).
- [14] V. T. Rajan, J. H. Lowenstein, and N. Andrei, *Phys. Rev. Lett.* **49**, 497 (1982).
- [15] K. Schotte and U. Schotte, *Phys. Lett. A* **55**, 38 (1975).
- [16] J. Ruvalds and Q. G. Sheng, *Phys. Rev. B* **37**, 1959 (1988).

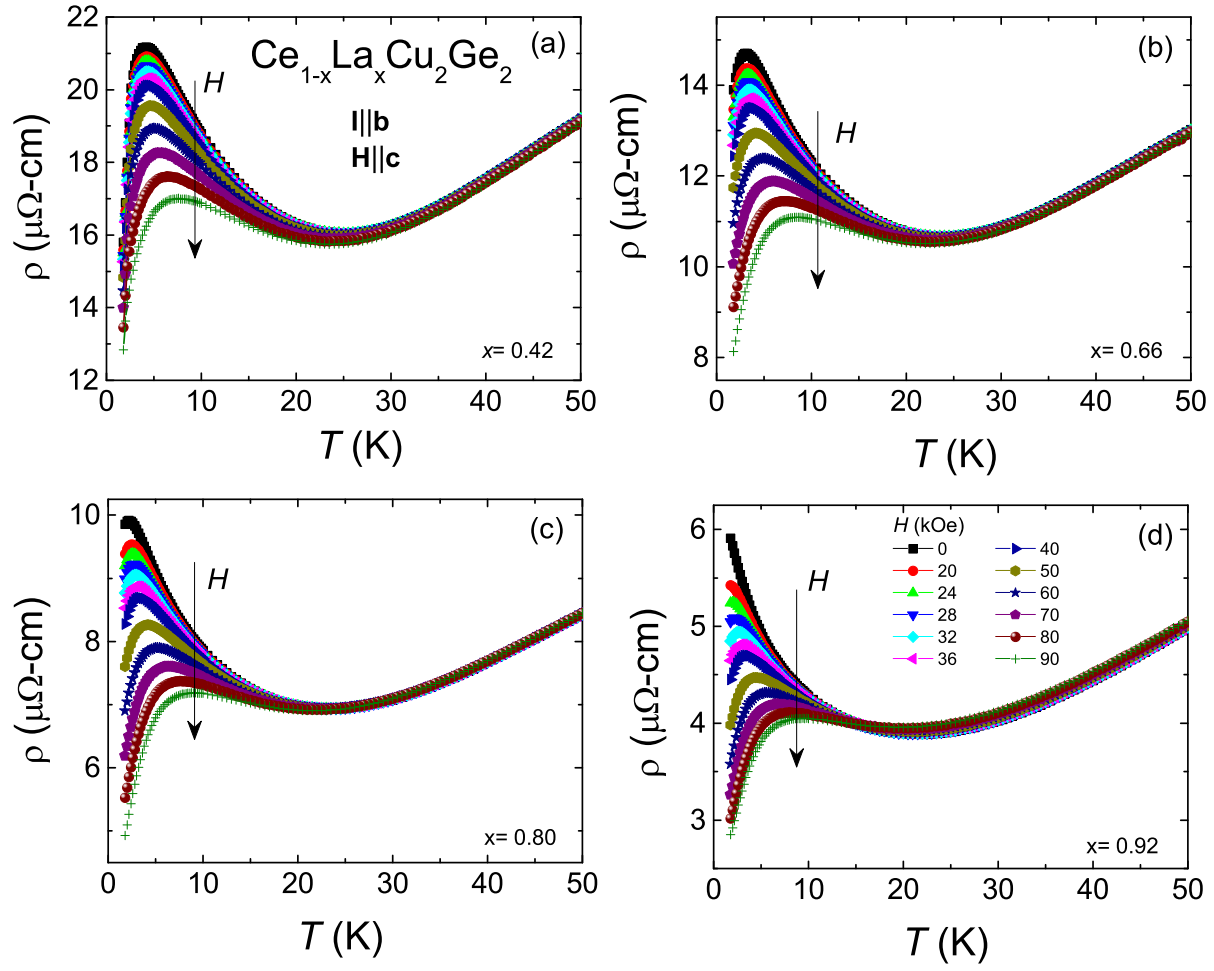


FIG. S9: Temperature-dependent resistivity data at constant magnetic fields with $\mathbf{H} \parallel \mathbf{c}$, for (a) $x = 0.425$, (b) $x = 0.66$, (c) $x = 0.80$, and (d) $x = 0.92$ ($\mathbf{I} \parallel \mathbf{b}$).